RESEARCH ARTICLE | JUNE 04 2025

The Langdon effect in laser plasmas: Absorption and conduction

Special Collection: Papers from the 66th Annual Meeting of the APS Division of Plasma Physics

N. R. Shaffer; T. Seo; S. X. Hu; V. N. Goncharov

Phys. Plasmas 32, 062703 (2025)
https://doi.org/10.1063/5.0266182

Physics of Plasmas ARTICLE pubs.aip.org/aip/pop

The Langdon effect in laser plasmas: Absorption and conduction

Cite as: Phys. Plasmas **32**, 062703 (2025); doi: 10.1063/5.0266182
Submitted: 17 February 2025 · Accepted: 7 May 2025 ·
Published Online: 4 June 2025

N. R. Shaffer,[1,a)] T. Seo,[1,2] S. X. Hu,[1,3,4] and V. N. Goncharov[1,4]

AFFILIATIONS

[1]Laboratory for Laser Energetics, University of Rochester, Rochester, New York 14623, USA
[2]Pittsford–Mendon High School, Pittsford, New York 14534, USA
[3]Department of Physics and Astronomy, University of Rochester, Rochester, New York 14623, USA
[4]Department of Mechanical Engineering, University of Rochester, Rochester, New York 14623, USA

Note: This paper is part of the Special Collection: Papers from the 66th Annual Meeting of the APS Division of Plasma Physics.
Note: Paper DI3 2, Bull. Am. Phys. Soc. **69** (2024).
[a)]Invited speaker. **Author to whom correspondence should be addressed:** nsha@lle.rochester.edu

ABSTRACT

A plasma heated by inverse bremsstrahlung absorption of laser light develops a non-Maxwellian electron distribution function, called the Langdon effect [A. B. Langdon, Phys. Rev. Lett. **44**, 575 (1980)]. These non-Maxwellian distributions are sufficiently long-lived to impact the absorption processes itself as well as the transport of heat by electrons. The theory of the Langdon effect in a homogeneous plasma is reviewed to clarify some aspects of Langdon's derivation as well as to confirm that the widely used super-Gaussian approximation works fairly well to describe the shape of the distribution function and reduction of the absorption rate. The Langdon effect on thermal conduction in an inhomogeneous plasma is developed by considering perturbations in a homogeneous absorbing plasma, which develops a heat flux due to both temperature and density gradients. A practical theory of the heat flux is developed by fitting the results of Vlasov–Fokker–Planck simulations, which avoids several approximations that compromised the usefulness of past theoretical predictions, most critically, the effect of electron–electron collisions on the fluxes. The present fits parameterize the coefficients of the temperature gradient (thermal conductivity) and the density gradient for a plasma of any ionization state and for any laser intensity where the theory of the Langdon effect remains locally valid. It is expected that this generalized theory of heat flow in an absorbing plasma will improve the predictive capability of radiation-hydrodynamics simulations of laser-produced plasmas, especially those formed in inertial confinement fusion experiments.

I. INTRODUCTION

Inverse bremsstrahlung (IB) absorption and thermal conduction are two fundamental processes governing the energetics and performance of laser-produced plasmas.[1] IB absorption converts the incident laser light into electron thermal energy, and conduction determines how that thermal energy is transported. In the context of inertial confinement fusion (ICF), correctly modeling both processes in radiation-hydrodynamics simulations is essential to the design and interpretation of experiments. In laser direct-drive ICF, the laser light is absorbed in the coronal plasma and conducted radially inward to drive an implosion.[2] The efficiency of the laser absorption and transport of energy to the ablation front are key to determining the overall drive efficiency. In indirect-drive ICF, the implosion is driven by x-rays emitted by the highly ionized *hohlraum* blowoff plasma.[3] The strength and symmetry of the drive depend on the electron density and temperature distribution inside the Marshak wave resulting from absorption and conduction in a complicated arrangement of overlapping laser beams. Outside of ICF, experiments on laser-heated gas-jet plasmas have provided valuable tests of fundamental laser-plasma interaction physics.[4–8] The thermodynamics of these plasmas is governed mainly by energy input via laser absorption and energy loss via heat conduction.[9]

The Langdon effect is one such laser-plasma phenomenon. It is the prediction that the electron distribution function will attain a long-lived non-Maxwellian shape in a plasma undergoing IB absorption.[10] In Langdon's original work, it was shown that this leads to a reduction in the IB absorption rate compared to a Maxwellian with increasing laser intensity. The effect is characterized by the parameter $\alpha = Zv_E^2/v_T^2$, where Z is the ion charge, $v_E = eE/(m_e\omega)$ is the oscillation speed of a free electron in an alternating electric field with amplitude E and angular frequency ω, and $v_T = \sqrt{k_B T/m_e}$ is the electron thermal velocity. Fokker–Planck simulations by Matte *et al.* showed that these non-Maxwellian distribution functions could be approximated by super-Gaussians, and they prescribed a relationship between α and the parameters of the super-Gaussian.[11] It has recently been experimentally verified that these non-Maxwellian distributions do occur and do reduce absorption.[6,7] The experimental confirmation of the Langdon effect renewed interest in producing accurate models for its effect on absorption suitable for radiation-hydrodynamic simulations.[8,12] A natural question is how the Langdon effect impacts other electron kinetic processes and whether these effects too can be distilled into simple models.

Such simple models will be especially valuable in mid- and high-Z plasmas, which can access modest to large values of α with realistic laser intensities and plasma temperatures. This is easiest seen by expressing $\alpha \approx 0.4Z\lambda_{\mu\mathrm{m}}^2 I_{15}/T_{keV}$, which relates it to the laser wavelength in microns, intensity in 10^{15} W/cm^2, and electron temperature in keV. This shows that any mid- or high-Z material ablated by an intense optical or ultraviolet laser should be expected to exhibit the Langdon effect to some degree. The preeminent example is the gold plasma produced by indirect-drive ICF experiments. However, directly driven glass (SiO_2) spheres used for basic plasma experiments also meet these criteria.[13,14] Another recently identified example is laser-driven extreme ultraviolet light sources, with applications to nanolithography.[15] There is evidently a wide range of laser-produced plasmas which could benefit from being able to predictively account for the Langdon effect.

The main new result of this work is a practical model for how the Langdon effect impacts electron thermal conduction. Modifications of the electron heat flux due to the Langdon effect have been investigated in many theoretical works over the past four decades, but none of these seem to have precipitated a model suitable for widespread adoption in radiation-hydrodynamics simulations. An early work by Mora and Yahi demonstrated the two main qualitative effects: a reduction in the thermal conductivity and the onset of a heat flux proportional to the electron density gradient.[16] Their calculations, however, involved two critical assumptions that limited their usefulness in practice. First, they neglected electron–electron collisions, which are essential in a quantitative theory of electron transport. Second, they assumed the unperturbed distribution function to be a super-Gaussian, but they offered no means of relating the shape of that super-Gaussian to the macrostate of the plasma, i.e., information that would be accessible in a radiation-hydrodynamics simulation. Mora and Yahi's work has been extended to include magnetization[17] and gradients in the super-Gaussian index,[18] but still without accurately treating electron–electron scattering. Maximov *et al.*[19] as well as Goncharov and Li[20] took a different approach by performing a Chapman–Enskog analysis, treating the laser electric field in the same order as the plasma gradients as perturbations to a local Maxwellian distribution. With this approach, they obtained novel ponderomotive contributions to the heat flux, but their heat flux lacks the expected density-gradient term and reduced thermal conductivity. Shaffer *et al.* used Vlasov–Fokker–Planck simulations to identify the reduction in the thermal conductivity without neglecting electron–electron collisions, but only a few values of Z were considered, and density gradients were not studied at all.[21] This work addresses both of these issues by providing a model for any Z based on Vlasov–Fokker–Planck simulations that predict both the thermal conductivity and density-gradient contributions to the heat flux for a plasma undergoing IB absorption.

In Sec. II, we first consider a homogenous plasma in some detail. This is important because a uniform absorbing plasma serves as the "equilibrium" situation for studying how the Langdon effect impacts conduction in an inhomogeneous plasma. We emphasize some subtle theoretical points that are often overlooked, identify analytic properties of the distribution function, and compare numerical solutions for the distribution function to the common super-Gaussian model. We also highlight the approximations made and potential areas for generalization. In Sec. III, the problem of the Langdon effect in heat conduction is taken up. After presenting some general features of the problem, the thermal conductivity work of Ref. 21 is extended by providing fits that can be evaluated at any values of Z and α. The contribution of density gradients is then considered, and new Vlasov–Fokker–Planck simulations are analyzed to provide a practical model for the density-gradient contribution to the heat flux.

II. INVERSE BREMSSTRAHLUNG ABSORPTION

Langdon's original work considered a homogeneous plasma in a high-frequency, low-amplitude laser field[10]

$$\mathbf{E}(t) = \mathrm{Re}\{\tilde{\mathbf{E}}e^{-i\omega t}\}. \tag{1}$$

The electrons respond to this field on both fast and slow timescales, which can be represented by the following ansatz for their distribution function:

$$f(\mathbf{v},t) = f_0(\mathbf{v},t) + \mathrm{Re}\left\{\tilde{f}(\mathbf{v},t)e^{-i\omega t}\right\}, \tag{2}$$

where it is assumed that the amplitudes f_0 and $\tilde{f}$ vary slowly in time compared to the laser oscillation. Two coupled kinetic equations result from collecting low- and high-frequency terms

$$\partial_t f_0 - \frac{e}{2m_e}\mathrm{Re}\left\{\tilde{\mathbf{E}}^* \cdot \partial_{\mathbf{v}}\tilde{f}\right\} = C_{ei}[f_0] + C_{ee}[f_0,f_0] + \frac{1}{2}\mathrm{Re}\left\{C_{ee}\left[\tilde{f}^*,\tilde{f}\right]\right\}, \tag{3}$$

$$\partial_t\tilde{f} - i\omega\tilde{f} - \frac{e}{m_e}\tilde{\mathbf{E}}\cdot\partial_{\mathbf{v}}f_0 = C_{ei}\left[\tilde{f}\right] + C_{ee}\left[\tilde{f},f_0\right] + C_{ee}\left[f_0,\tilde{f}\right], \tag{4}$$

where C_{ei} and C_{ee} are collision operators for electron–ion and electron–electron scattering, respectively.

Langdon's theory may be obtained from neglecting the explicit time dependence of $\tilde{f}$, neglecting electron–electron collision terms involving $\tilde{f}$, assuming f_0 is an isotropic function of velocity, and taking C_{ei} to be an elastic pitch-angle scattering operator. One finds

$$\tilde{f} = \frac{\nu_{ei} + i\omega}{[\nu_{ei}(v)]^2 + \omega^2}\frac{e\tilde{\mathbf{E}}\cdot\mathbf{v}}{m_e v}\partial_v f_0, \tag{5}$$

where

$$\nu_{ei}(v) = 4\pi\left(\frac{e^2}{4\pi\epsilon_0 m_e}\right)^2\frac{\sum_j Z_j^2 n_j \Lambda_{ej}}{v^3} \tag{6}$$

is the electron–ion scattering rate, which involves a sum over all ion species with charge number Z_j, density n_j, and Coulomb logarithm

Λ_{ej}, which may depend on velocity in general. Eliminating $\tilde{f}$ from the f_0 equation yields

$$\partial_t f_0 = \frac{v_E^2}{6v^2}\partial_v\left[v^2\nu_{ei}(v)g(v)\partial_v f_0\right] + C_{ee}[f_0, f_0], \tag{7}$$

where $v_E = e|\tilde{\mathbf{E}}|/(m_e\omega)$ is the electron quiver speed. The function $g(v) = [1+\nu_{ei}^2(v)/\omega^2]^{-1}$ sharply transitions from zero at low velocities to unity at high velocities. The transition happens where $\nu_{ei}(v) = \omega$, which is typically a very low velocity. For a thermal velocity electron, it follows that

$$\frac{\nu_{ei}(v_T)}{\omega} = \sqrt{\frac{n_e}{n_{\text{crit}}}}\frac{\sum_j Z_j{}^2 n_j\Lambda_{ej}}{\sum_j Z_j n_j}\frac{1}{4\pi n_e\lambda_{De}^3}, \tag{8}$$

where $n_{\text{crit}} = \epsilon_0 m_e\omega^2/e^2$ is the critical density of the laser, and $\lambda_{De} = \sqrt{\epsilon_0 k_B T_e/(e^2 n_e)}$ is the electron Debye length. Thus, for any plasma that is underdense ($n_e < n_{\text{crit}}$) and weakly coupled ($n_e\lambda_{De}^3 \gg 1$), the function $g(v)$ will be different from unity only for $v \ll v_T$. For this reason, the theory that follows will take $g(v)\approx 1$; the ramifications will be discussed at the end of the section.

The interpretation of the right-hand side of Eq. (7) is straightforward. The first term represents IB absorption of the laser light, which tends to drive f_0 away from a Maxwell–Boltzmann distribution. This is impeded by electron–electron collisions, which drive f_0 toward a Maxwell–Boltzmann distribution. Since both electron–electron collisions and IB absorption are diffusion operators in velocity space, the balance between the two is given by the ratio of their characteristic diffusion coefficients. For electron–electron collisions, this is, $v_T^2\nu_{ee}(v_T)$, where $\nu_{ee}(v_T) = 4\pi\left(\frac{e^2}{4\pi\epsilon_0 m_e}\right)^2\frac{n_e\Lambda_{ee}}{v_T^3}$ is the electron–electron collision rate with Coulomb logarithm Λ_{ee}. For IB absorption, the diffusion coefficient is $v_E^2\nu_{ei}(v_T)$. The ratio of the two is

$$\frac{v_E^2\nu_{ei}(v_T)}{v_T^2\nu_{ee}(v_T)} = Z\frac{v_E^2}{v_T^2} = \alpha, \tag{9}$$

where $Z = \frac{\sum_j Z_j^2 n_j\Lambda_{ej}}{n_e\Lambda_{ee}}$ is an effective ion charge.

While the shape of f_0 varies in time, so too does the temperature

$$k_B\partial_t T_e = -\frac{2\pi m_e v_E^2}{9n_e}\int_0^\infty v^3\nu_{ei}(v)g(v)\partial_v f_0 \mathrm{d}v, \tag{10}$$

$$\approx \frac{2\pi}{9}m_e v_E^2\nu_{ei}(v_T)\frac{v_T^3}{n_e}f_0(0,t), \tag{11}$$

where the second line follows by setting $g(v)$ equal to unity and neglecting any velocity dependence in the Coulomb logarithm. Since the temperature increases monotonically, there are no true steady-state solutions of Eq. (7); however, there do exist quasi-steady *normal* solutions, defined as being solutions where f_0 depends on time only implicitly via the temperature.[22] This is realized by the change of variables[23]

$$x = v/v_T(t) \quad f_0(v,t) = \frac{n_e}{(2\pi)^{\frac{3}{2}}v_T^3(t)}\phi(x). \tag{12}$$

Since this ansatz scales out the density and temperature dependence of the distribution function, the definitions of these two moments produce two consistency conditions on $\phi(x)$

$$\begin{pmatrix} n_e \\ 3n_e T_e(t)\end{pmatrix} = 4\pi\int_0^\infty\begin{pmatrix} v^2 \\ m_e v^4\end{pmatrix}f_0(v,t)\mathrm{d}v$$
$$\Rightarrow \sqrt{\frac{2}{\pi}}\int_0^\infty\begin{pmatrix} x^2 \\ x^4\end{pmatrix}\phi(x)\mathrm{d}x = \begin{pmatrix} 1 \\ 3\end{pmatrix}. \tag{13}$$

When a Fokker–Planck collision operator is used for C_{ee}, the time-dependent kinetic equation for $f_0(v,t)$ may be reduced to a univariate integro-differential equation for $\phi(x)$

$$0 = \phi(x)A(x) + \phi'(x)B(x), \tag{14}$$

$$A(x) = I_0(x) + \frac{\alpha}{18}\sqrt{\frac{\pi}{2}}\phi(0)x^3, \tag{15}$$

$$B(x) = \frac{x}{3}[I_2(x) + J_{-1}(x)] + \frac{\alpha}{6x}, \tag{16}$$

where

$$x^r I_r(x) = \sqrt{\frac{2}{\pi}}\int_0^x y^{r+2}\phi(y)\mathrm{d}y, \tag{17}$$

$$x^r J_r(x) = \sqrt{\frac{2}{\pi}}\int_x^\infty y^{r+2}\phi(y)\mathrm{d}y \tag{18}$$

are integral operators arising from the electron–electron collision operator for an isotropic distribution.[24,25] To arrive at Eq. (14), from Eq. (7), one first must eliminate the time derivative using the chain rule and Eq. (11). This produces a second-order integro-differential equation, which may be integrated once to produce the first-order equation, Eq. (14).

A simple way to solve Eq. (14) is to set up an iteration

$$\phi_{n+1}(x) = \phi_{n+1}(0)\exp\left[-\int_0^x\frac{A_n(y)}{B_n(y)}\mathrm{d}y\right], \tag{19}$$

where A_n and B_n are evaluated using the current estimate $\phi_n(x)$. During the iteration, $\phi_n(x)$ may not exactly respect the consistency conditions Eq. (13), but these may be restored by rescaling ϕ_n and x after each iteration.

Some basic features of the distribution can be obtained by analysis of the low- and high-velocity limits. The limiting behavior of the A and B functions as $x\to 0$ follows from Taylor series expansion of the integrals $I_0(x)$, $I_2(x)$, and $J_{-1}(x)$. The results are

$$A(x) = \frac{1}{3}\sqrt{\frac{2}{\pi}}\left(1+\frac{\alpha}{6}\right)\phi(0)x^3 + O(x^5), \tag{20}$$

$$B(x) = \frac{\alpha}{6x} + O(x^2), \tag{21}$$

which implies that for velocities less than the thermal speed, the shape of the distribution function is

$$\phi(x)\approx\phi(0)\exp\left[-\frac{1}{15}\sqrt{\frac{2}{\pi}}\left(1+\frac{6}{\alpha}\right)\phi(0)x^5\right]. \tag{22}$$

The singular behavior at $\alpha = 0$ results from replacing the function $g(v)$ with unity. This is not an issue, since the $\alpha = 0$ solution is a Maxwellian. The limiting behavior as $x\to\infty$ is obtained by taking the integration limits in $I_0(x)$, $I_2(x)$, and

$J_{-1}(x)$ to be infinity and using the consistency conditions, Eq. (13). Doing so yields

$$A(x) \sim 1 + \frac{\alpha}{18}\sqrt{\frac{2}{\pi}}\phi(0)x^3, \tag{23}$$

$$B(x) \sim \left(1 + \frac{\alpha}{6}\right)\frac{1}{x}, \tag{24}$$

which imply that for velocities much larger than the thermal speed, the shape of the distribution function is

$$\phi(x) \sim \phi(0)\exp\left[-\frac{x^2 + \frac{\alpha}{45}\sqrt{\frac{2}{\pi}}\phi(0)x^5}{2\left(1+\frac{\alpha}{6}\right)}\right]. \tag{25}$$

Observe that as $\alpha \to \infty$, the small- and large-x limits coalesce into

$$\phi(x) = \phi(0)\exp\left[-\frac{1}{15}\sqrt{\frac{2}{\pi}}\phi(0)x^5\right], \tag{26}$$

which is the exact solution of Eq. (14) in this limit.

Numerical solutions of Eq. (14) are shown in Fig. 1, which also compares them to the widely used super-Gaussian parameterization by Matte *et al.*[11]

$$\phi_m(x) = c_m \exp\left[-(x/x_m)^m\right], \tag{27}$$

$$x_m = \sqrt{\frac{3\Gamma(3/m)}{\Gamma(5/m)}}, \tag{28}$$

$$c_m = \sqrt{\frac{\pi}{2}}\frac{m}{\Gamma(3/m)x_m^3}. \tag{29}$$

The exponent of the super-Gaussian is prescribed to be

$$m(\alpha) = 2 + \frac{3}{1 + 1.66\alpha^{-0.724}}, \tag{30}$$

which interpolates between the analytic limits $m(0) = 2$ and $m(\infty) = 5$. Matte *et al.* determined the numerical coefficients by fitting to time-dependent solutions of Eq. (7) rather than by parameterizing the normal solutions. Nevertheless, Fig. 1 demonstrates that their fits reproduce the normal solutions very well overall. A notable exception is intermediate values of α, where the low-velocity part of the distribution is somewhat underestimated. This leads to an overestimate of the tail population, since normalization must be preserved.

In spite of its imperfections, the super-Gaussian parameterization is very accurate for describing how the IB absorption rate is impacted by a non-Maxwellian distribution. In Langdon's theory, the fractional reduction is simply $\phi(0)$, which is plotted in Fig. 2 for both the numerical normal solutions and the super-Gaussian model. The two are difficult to distinguish.

Langdon's theory[10] and Matte *et al.*'s model[11] for the distribution function and absorption rate are attractive in their simplicity. For the remainder of this work, they are taken to be an adequate local description of laser absorption and its kinetic effects on the electron distribution function. That said, there are several caveats worth mentioning. Some of these are minor approximations in the above theory that may easily be relaxed when necessary. Others are more difficult theoretical

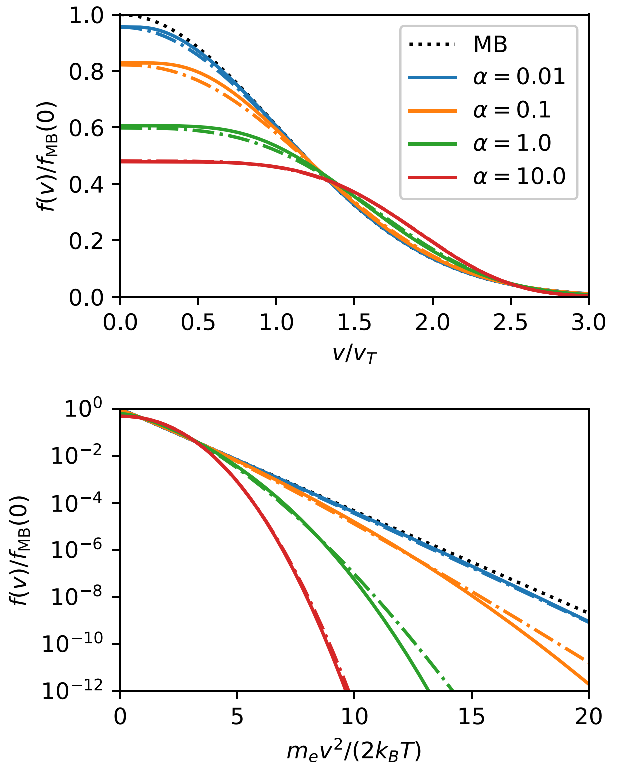

FIG. 1. Distribution function of a homogenous plasma undergoing IB absorption. Upper: focus on the low-velocity component relevant to the absorption rate. Lower: focus on the high-energy tails relevant to conduction. Black dotted curves are a Maxwellian distribution. Solid curves are solutions to Eq. (14). Dashed curves are the super-Gaussian model of Matte *et al.*[11]

questions which are interesting, if not immediately relevant to the rest of the present work.

First, the direct relationship between the absorption rate and the zero-velocity value of the distribution function is quite special. It holds

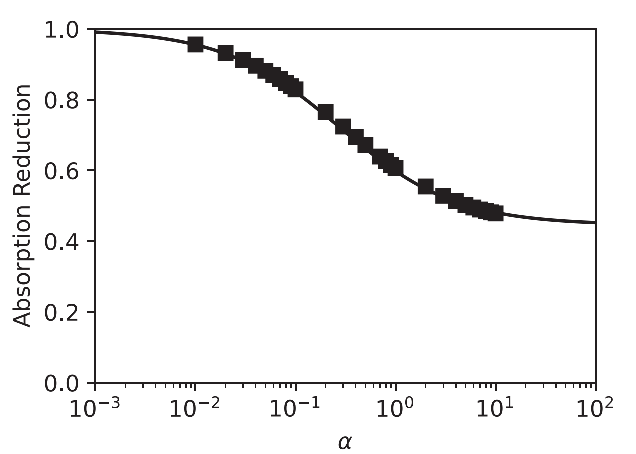

FIG. 2. Absorption rate reduction factor. Squares are the numerical solutions to Eq. (14). The solid curve is derived from the super-Gaussian model of Matte *et al.*[11]

only when the electron–ion collision rate has exactly a v^{-3} dependent on velocity. Sherlock *et al.* recently revisited the calculation of the absorption rate reduction, taking into account more realistic velocity dependence in the Coulomb logarithm.[12] They found a slightly milder reduction of the absorption rate at intermediate α compared to Langdon's theory and provided practical interpolation formulas for their results.

Second, replacing the function $g(v)$ with unity breaks down at velocities where $\nu_{ei}(v) > \omega$. This corresponds to electrons that cannot even complete one oscillation in the laser field before scattering off an ion. Accounting for this effect in numerical solutions for $\phi(x)$ involves modifying the function $B(x)$, which causes the small-x dependence of $\phi(x)$ to develop a Maxwellian boundary layer that abruptly transitions to Eq. (22). For the low densities, high temperatures, and short wavelengths typical of laser absorption in current ICF experiments, this boundary layer is so narrow that it may be safely neglected for most practical purposes. For example, if one is interested in positive moments of f (e.g., density, temperature, currents), the subthermal velocities make little contribution, and so a small error in the distribution function at these velocities has no impact.

Third, Langdon's theory assumes that the slowly varying component of the distribution function is isotropic. However, the laser accelerates each electron in the direction of the laser polarization. If the amplitude of the oscillatory motion is comparable to the random thermal motion, then the parallel and perpendicular components of the electron's motion will damp at different rates and give rise to a slowly varying anisotropy.[26–30] This anisotropy not only affects the heating rate but also can lead to unequal temperatures in the parallel and perpendicular directions.[31–33] The characteristic parameter for these strong-field effects is v_E^2/v_T^2. In typical ICF experiments, these are not a major concern relative to the Langdon effect, since IB absorption mainly happens via relatively highly charged ions (carbon for direct-drive and gold for indirect-drive).

Fourth, there are unresolved questions about whether Langdon's theory adequately accounts for electron–electron collisions. Recall that in order to obtain Eq. (7), electron–electron scattering terms involving the high-frequency response of the electrons were neglected. Fourkal *et al.* reported particle-in-cell simulation results showing Maxwellian tails in the distribution function that are not predicted by Langdon's theory.[23] They also derived (but did not solve) a kinetic equation like Eq. (14) with additional electron–electron collision terms. We were not able to find a stable method of solving that equation to verify if it indeed produces a Maxwellian tail. That equation involves third-order derivatives, and it can be shown that near $x = 0$, one of its three general solutions diverges like $e^{\frac{1}{\sqrt{x}}}$. It appears that numerical solutions are prone to getting polluted by the divergent mode, which causes the whole solution to blow up, even when implicit integrators with nominally excellent stability properties are used. Even if a solution could be obtained, there is the further complicating matter that these additional terms are of order v_E^2/v_T^2. It stands to reason that once they become relevant, so too should be the above-mentioned anisotropy effects. Nevertheless, it would be very valuable to solve the issue of numerical instability so that the hypothesis of Maxwellian tails can be either supported or refuted.

III. ELECTRON HEAT FLOW

A. Basic theory and thermal conductivity

After accepting that the "equilibrium" distribution function for a laser-absorbing plasma is non-Maxwellian, the immediate question is how transport processes are affected when the plasma is inhomogeneous. In unmagnetized laser fusion, electron thermal conduction is the most important of these processes. We consider a slightly inhomogeneous plasma, meaning that the temperature and density gradients have a long length scale compared to the electron collision mean free path.

In the absence of any gradients, the distribution function is isotropic, so their inclusion will induce a weak anisotropy

$$f(\mathbf{x}, \mathbf{v}, t) = f_0(\mathbf{x}, v, t) + \frac{\mathbf{v}}{v} \cdot \mathbf{f}_1(\mathbf{x}, v, t). \tag{31}$$

The induced electric and energy current densities, $\mathbf{J}$ and $\mathbf{Q}$, respectively, are moments of $\mathbf{f}_1$

$$(\mathbf{J}, \mathbf{Q}) = \frac{4\pi}{3}\int_0^\infty \left(-e, \frac{1}{2}m_e v^2\right) v^3 \mathbf{f}_1(v)\mathrm{d}v. \tag{32}$$

The two components of the distribution function satisfy the kinetic equations

$$\partial_t f_0 + \frac{v}{3}\nabla\cdot\mathbf{f}_1 - \frac{e}{3m_e v^2}\partial_v(v^2\mathbf{E}\cdot\mathbf{f}_1) = C_0 + C_{\mathrm{IB}}, \tag{33}$$

$$\partial_t \mathbf{f}_1 + v\nabla f_0 - \frac{e}{m_e}\mathbf{E}\partial_v f_0 = -\nu_{ei}(v)\mathbf{f}_1 + \mathbf{C}_1, \tag{34}$$

where $\mathbf{E}$ is a quasi-static electric field, C_0 and $\mathbf{C}_1$ are, respectively, the isotropic and anisotropic projections of the electron–electron collision operator, and C_{IB} is the absorption operator from Eq. (7). Note that by coupling the transport processes and IB absorption in this way, we are assuming that the transport processes take place on a time scale that—like the IB heating time scale—is much longer than that of the laser oscillation. If $\mathbf{f}_1$ is a small perturbation like the gradients and quasi-static field, then it may be neglected in the kinetic equation for f_0

$$\partial_t f_0 = C_0 + C_{\mathrm{IB}}, \tag{35}$$

which is just Eq. (7) describing the shape of f_0 according to the local value of α. Assuming that $\mathbf{f}_1$ varies in time only implicitly via f_0, we may take $\partial_t\mathbf{f}_1 = 0$ and apply the chain rule to obtain

$$\mathbf{f}_1 - \nu_{ei}^{-1}\mathbf{C}_1 = -\lambda_{ei}\left[\frac{\partial f_0}{\partial n_e}\nabla n_e + \frac{\partial f_0}{\partial T}\nabla T - \frac{e}{m_e v}\frac{\partial f_0}{\partial v}\mathbf{E}\right], \tag{36}$$

where $\lambda_{ei} = v/\nu_{ei}$ is the electron–ion collision path.

For a fixed model of f_0—for example, a super-Gaussian—one could solve Eq. (36) to obtain the components of $\mathbf{f}_1$, treating ∇n_e, ∇T, and $\mathbf{E}$ as linearly independent. Evaluating the moments $\mathbf{J}$ and $\mathbf{Q}$ then allows for identifying the transport coefficients. In an unmagnetized plasma, one typically imposes a $\mathbf{J} = 0$ quasi-neutrality condition. This allows for eliminating the electric field from the energy current, which can then be identified as the proper heat flux. The general form will be

$$\mathbf{Q} = -\kappa\nabla T + \mu\nabla n_e. \tag{37}$$

The first term corresponds to the usual Fourier heat law, while the second one is unusual. When f_0 is Maxwellian, one finds always that

$\mu = 0$ and only Fourier's law remains. However, if there is some means of sustaining a non-Maxwellian "equilibrium," then μ will be nonzero. In the current work, we are concerned with laser absorption only, but a similar situation arises anytime there is some non-elastic collision process affecting f_0, as in granular gases.[34]

The only technical difficulty in determining the transport coefficients is the inversion of the electron–electron collision operator $\mathbf{C}_1$. In the Lorentz approximation, this term is neglected, and the transport coefficients for a super-Gaussian f_0 may be found analytically to be[16]

$$\frac{\kappa_m}{\kappa_2} = \frac{a_m(7b_m - 5c_m)}{a_2(7b_2 - 5c_2)}, \tag{38}$$

$$\frac{n_e\mu_m}{T\kappa_2} = -\frac{2a_m(b_m - c_m)}{a_2(7b_2 - 5c_2)}, \tag{39}$$

where

$$\kappa_2 = \frac{128}{\sqrt{2\pi}}\frac{n_e k_B^2 T}{m_e \nu_{ei}(v_T)} \tag{40}$$

is the Maxwellian limit, and the parameters of the super-Gaussian corrections are $a_m = [\Gamma(3/m)]^{\frac{5}{2}}[3/\Gamma(5/m)]^{\frac{7}{2}}$, $b_m = \Gamma(10/m)/12$, and $c_m = [\Gamma(8/m)]^2/[9\Gamma(6/m)]$. Here, m is the super-Gaussian exponent, as in Eq. (27). One can confirm that the coefficient μ vanishes for a Maxwellian.

Spitzer and Härm carried out numerical solutions of Eq. (36) for a Maxwellian f_0 and obtained numerical correction to κ_2 at several values of Z.[35] One widely used parameterization of this electron–electron collision correction is[36]

$$\kappa_{\mathrm{SH}} = \kappa_2 \frac{Z + 0.24}{Z + 4.2}, \tag{41}$$

which shows that the Lorentz limit, κ_2, is approached quite slowly as $Z \to \infty$ and is wrong by about a factor of four for hydrogen.

An analogous solution of Eq. (36) for either super-Gaussians or the normal solutions discussed in Sec. II has not been carried out to date. However, time-dependent Vlasov–Fokker–Planck solutions of Eqs. (33) and (34) were recently used to obtain corrections to the Spitzer–Härm thermal conductivity as a function of α.[21] These involved simulating the decay of a sinusoidal temperature perturbation in a plasma being uniformly heated by a laser with a fixed intensity. The α dependence of the correction was fitted to

$$\frac{\kappa}{\kappa_{\mathrm{SH}}} = \frac{c_0(Z) + c_1(Z)\alpha}{1 + c_2(Z)\alpha}, \tag{42}$$

and the coefficients were tabulated for $Z = 1, 3.5, 10, 29, 80$. To complete the model, we provide here interpolation formulas for the Z dependence of these coefficients

$$\begin{aligned} &c_k(Z) = p_k Z^{-q_k} \quad (k = 0, 1, 2),\\ &p_0 = 0.986 \quad p_1 = 1.327 \quad p_2 = 4.961,\\ &q_0 = 0.003 \quad q_1 = 0.171 \quad q_2 = 0.147. \end{aligned} \tag{43}$$

Since the Z dependence is quite weak, these formulas should extrapolate to $Z > 80$ in a sensible way. In Fig. 3, the accuracy of the interpolation is checked by plotting Eq. (42) with c_k taken either from the tabulated values in Ref. 21 or using the interpolation formula Eq. (43).

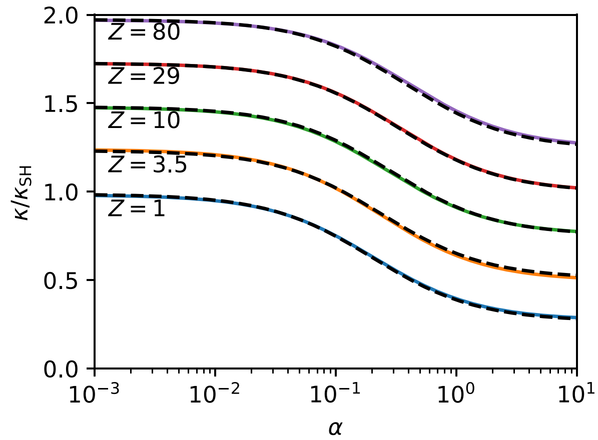

FIG. 3. Comparison of interpolation formulas for the thermal conductivity. Solid curves are the fits to Vlasov–Fokker–Planck simulations using Eq. (42) at specific values of Z. Dashed curves are the parameterization of the Z dependence, Eq. (43), evaluated at the same values of Z to check the accuracy of the Z interpolation. Curves are shifted by multiples of 0.25 for clarity.

Note that each curve is shifted for clarity. The interpolation is seen to be quite accurate, thanks to the very weak Z dependence of the model.

B. Density gradients

Obtaining the density-gradient coefficient from time-dependent simulations is more challenging. The reason is that when a density gradient is superposed on a uniform and isothermal plasma, regions of higher density will absorb more rapidly than those of lower density. One thus ends up with a temperature gradient that is perfectly correlated with the density gradient. For example, in the case of a sinusoidal density perturbation, the temperature perturbation will be perfectly in phase, preventing any direct identification of their separate contributions to the heat flux. Our approach to isolating the density-gradient contribution is to rely on Eq. (42) to model the temperature-gradient contribution and subtract it from the total heat flux. This is not ideal, because the temperature-gradient contribution is expected to be a significant part of the total heat flux, so errors in the model for κ will propagate to the determination of μ in a way that is difficult to quantify. Further, the normalized coefficient $n_e\mu/(T\kappa_{\mathrm{SH}})$ is smaller in magnitude than $\kappa/\kappa_{\mathrm{SH}}$, so small relative errors in the model for κ can become large relative errors in the determination of μ.

Despite these difficulties, we were able to obtain high-quality simulation results for $Z < 10$ as well as $Z = \infty$. As in Ref. 21, the *K2* Vlasov–Fokker–Planck code was used to simulate sinusoidal perturbations in a linear simulation domain with periodic boundary conditions.[37] The domain size was $L = 1$ mm, divided equally into 96 cells. The electrons were initialized to be locally Maxwellian with a temperature of 200 eV and a density profile $n_e(x) = 1.46 \times 10^{21}\mathrm{cm}^{-3}[1 + 10^{-3}\cos(2\pi x/L)]$. The velocity grid extended to 15 times the initial thermal speed and used 200 equal-sized cells. The laser wavelength was 351 nm, and its intensity varied from 10^{12} to 5×10^{15} W/cm^2. The instantaneous value of μ was obtained from the heat flux Q_x as

$$\mu = \frac{1}{L}\int_0^L \frac{Q_x + \kappa\partial_x T}{\partial_x n_e}\,\mathrm{d}x, \tag{44}$$

where κ was obtained using Eq. (42). Only a small window of time was useful for obtaining μ. At early times, there is a transient as the initial Maxwellian relaxes to the correct distribution, which lasts 1–2 ps at the chosen conditions. At later times, the rapid heating of the electrons causes truncation errors in velocity space when the initial grid can no longer contain the distribution function of the heated electrons. This happens quite rapidly at high Z and prevented obtaining useful results for $Z > 10$ or higher intensity. For this reason, only the regime $\alpha \lesssim 1$ could be assessed in this work.

To select the window of time corresponding to reliable simulation data, we filtered based on two requirements. The first is that $T(t) < 1250\,\mathrm{eV}$, which removes data at late times where too much heating has occurred, causing truncation errors in velocity space. The value 1250 eV corresponds to the temperature at which the highest velocity grid point is equal to $6v_T(t)$. The second requirement is that running the same simulation at two different mean densities yields consistent values for $n_e\mu/(T\kappa_{\mathrm{SH}})$, which must be independent of density. We found that a good heuristic for this is to inspect $\Delta T/T$, the instantaneous ratio of the temperature perturbation amplitude to its mean value. This is illustrated in the upper panel of Fig. 4, where each

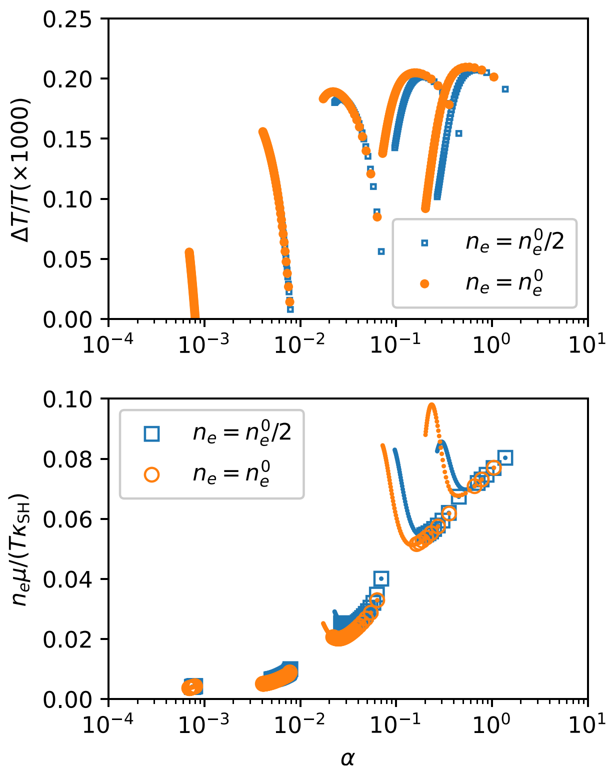

FIG. 4. Typical results for a density-perturbation simulation, shown here for $Z = 3.5$ and two different densities: $n_e^0 = 1.46\times10^{21}\,\mathrm{cm}^{-3}$ (orange) and $n_e^0/2$ (blue). In both panels, each track of points corresponds to a simulation with a different laser intensity (increasing from left to right). Upper panel: heuristic for determining consistency at different densities. Lower panel: full simulation results (small symbols) and downselected results (large open symbols).

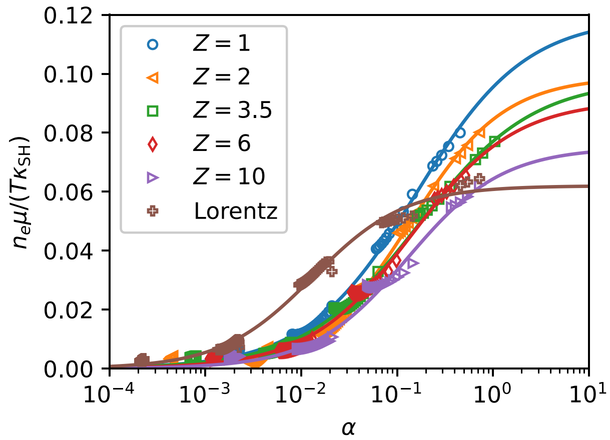

FIG. 5. Density gradient coefficient of the heat flux as a function of α for various Z, as well as for a Lorentzian plasma. Symbols are Vlasov–Fokker–Planck simulation results. Lines are fits based on Eq. (45).

track of points comes from a simulation with a different laser intensity. Whenever $\Delta T/T$ is a decreasing function of α (increasing function of time), calculations at different densities are in agreement. The lower panel of Fig. 4 shows how the two requirements are used to downselect the data used for further analysis. The small markers are the instantaneous values of $n_e\mu/(T\kappa_{\mathrm{SH}})$ and α for the whole simulation; those that satisfied both requirements above were marked with larger open symbols. These are the ones retained in the analysis below.

The Vlasov–Fokker–Planck results for μ are plotted in Fig. 5, together with analytic fits. The fits are parameterized as

$$\frac{n_e\mu}{T\kappa_{\mathrm{SH}}} = \frac{b_0(Z)}{1 + b_1(Z)\alpha^{-b_2(Z)}}, \tag{45}$$

which interpolates between zero as $\alpha \to 0$ and b_0 as $\alpha \to \infty$. Coefficients are listed in Table I. It is interesting that compared to the thermal conductivity, $\kappa/\kappa_{\mathrm{SH}}$, the density gradient coefficient appears to have a stronger Z dependence. This indicates that electron–electron scattering, specifically the operator $\mathbf{C}_1$ of Eq. (34), is quite important for accurately determining μ. Another indication of the importance of electron–electron collisions is that there does not seem to be a convergence toward the Lorentz limit with increasing Z, except as $\alpha \to \infty$. This was also seen in the thermal conductivity and is due to the unphysical nature of taking $Z \to \infty$ but keeping α finite.[21] Only in the limit where both Z and α go to infinity does the Lorentz limit make

TABLE I. Fit parameters for the density gradient coefficient, as in Eq. (45).

Z	b_0	b_1	b_2
1	0.119	0.247	0.760
2	0.099	0.172	0.887
3.5	0.098	0.272	0.734
6	0.091	0.208	0.807
10	0.075	0.166	0.876
∞	0.062	0.020	0.904

sense. This is further supported by our Lorentz plasma simulation results, which extrapolate to $n_e\mu/(T\kappa_{\rm SH}) \to 0.062$ as $\alpha \to \infty$, which is in fairly good agreement with the value 0.066 expected for an $m = 5$ super-Gaussian.

In order to interpolate these results at arbitrary Z, we propose the following formulas for the coefficients b_k:

$$b_k(Z) = \frac{r_k + b_k(\infty)s_kZ}{1 + s_kZ} \quad (k = 0, 1, 2), \tag{46}$$

where $b_k(\infty)$ are the limiting values in Table I, and

$$\begin{array}{lll} r_0 = 0.136 & r_1 = 0.240 & r_2 = 0.754 \\ s_0 = 0.351 & s_1 = 0.037 & s_2 = 0.085 \end{array}$$

are the fit parameters. The use of the Lorentz limit helps to constrain the model to produce sensible values even for $Z > 10$, where Vlasov–Fokker–Planck results were not obtained. The accuracy of this interpolation is checked in Fig. 6, which compares the predictions of Eq. (45) using values of b_k obtained either from Table I or Eq. (46). While not perfect, the Z-interpolation should be accurate enough to be able to assess the effect of density gradients on the heat flow in integrated radiation-hydrodynamic simulations of laser-produced plasmas.

IV. DISCUSSION AND OUTLOOK

This work is concerned entirely with the local theory of absorption and transport due to small departures from that homogeneous state. It should be acknowledged, however, that sharp gradients do occur in many laser-produced plasmas, and the local theory of heat flow breaks down. In this situation, hydrodynamic modeling must appeal to non-local electron conduction models, which typically take the form of flux-limiting schemes,[38] convolution approximations,[39] or reduced kinetic models.[40–43] In either situation, the local electron heat flux often remains a key ingredient. The results of Sec. III show that it should be modified in absorbing regions to account for the α dependence of the thermal conductivity as well as the novel effect of electron density gradients.

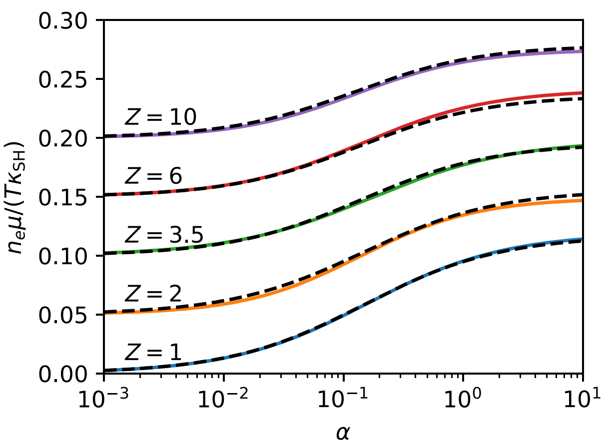

FIG. 6. Comparison of interpolation formulas for the density gradient coefficient of the heat flux. Solid curves are the fits to Vlasov–Fokker–Planck simulations using Eq. (45) at specific values of Z. Dashed curves are the parameterization of the Z dependence, Eq. (46), evaluated at the same values of Z to check the accuracy of the Z interpolation. Curves are shifted by multiples of 0.05 for clarity.

One important detail is that the theory of conduction presented here is predicated on Langdon's theory being a good representation of the local state of the plasma. In Sec. II, we listed some scenarios where Langdon's theory may not be reliable, for example, if $v_E \sim v_T$. The practical formulas we propose will still produce finite, plausible answers in these cases, though one cannot be entirely sure that they are still quantitatively accurate. Another situation which requires caution is that of very short laser pulses. If the intensity of the laser varies on a timescale that is shorter than the electron–ion collision time, then the absorption and conduction processes are transient and kinetic. In this case, the evolution of the electron distribution function cannot be understood using the normal solution method used here.

Since the Langdon effect concerns changes to the electron distribution function, its impact is not limited to absorption and conduction; all aspects of electron kinetics are affected in principle. Two processes of special experimental interest are x-ray emission and ionization kinetics.

The emission of x-rays was studied by Matte *et al.*[11] within the super-Gaussian approximation, but as shown in this work, the tails of the distribution function are not correct in this model for moderate values of α. Further, that work did not consider the full velocity dependence of the emission Gaunt factor. It should be straightforward to revisit the Langdon effect on x-ray emission using the normal solutions of Eq. (14) and a detailed treatment of the bremsstrahlung Gaunt factor, similar to Refs. 8 and 12. Another interesting question for future consideration is if the emission of these x-rays could happen rapidly enough to modify the temperature balance of Eq. (11). In this work, we have assumed that the laser absorption process occurs on a sufficiently rapid time scale to neglect all other heating or cooling mechanisms for the purposes of determining the shape of the distribution function. If this breaks down, then the development of the normal solution method here would have to be extended to account for these other thermodynamic processes.

The interplay between ionization kinetics with the Langdon effect is a more complex problem. On the one hand, it should be straightforward to evaluate how the relevant ionization, excitation, and recombination cross sections are modified by the Langdon effect. However, it was shown by Le *et al.*[44] using Vlasov–Fokker–Planck simulations coupled to atomic rate equations that the ionization and recombination themselves can influence the shape of the distribution function. Since the various atomic rates introduce additional material-dependent timescales, it seems unlikely that the interplay of ionization kinetics with the Langdon effect can be reduced to a simple model like those developed in the present work.

In summary, we have reviewed the theory of the Langdon effect as it pertains to IB absorption. Taking the resulting distribution function as the local "equilibrium," we have provided the first comprehensive quantitative theories of how the Langdon effect impacts heat conduction in unmagnetized plasmas. The results of Vlasov–Fokker–Planck simulations have been parameterized in a simple way that should aid in the adoption of this model in radiation-hydrodynamics simulation codes.

ACKNOWLEDGMENTS

This work was supported by the Department of Energy [National Nuclear Security Administration] University of Rochester "National Inertial Confinement Fusion Program" (Award No. DE-NA0004144).

The authors wish to thank Mark Sherlock for support using the *K*2 code, R. Steven Craxton for directing the LLE Summer High School Program, as well as Andrei Maximov, David Strozzi, and Hai Le for useful discussions relating to this work.

AUTHOR DECLARATIONS

Conflict of Interest

The authors have no conflicts to disclose.

Author Contributions

Nathaniel R. Shaffer: Conceptualization (lead); Data curation (equal); Investigation (lead); Methodology (lead); Project administration (equal); Supervision (equal); Visualization (equal); Writing – original draft (lead). **Timothy Seo:** Data curation (equal); Investigation (equal); Validation (equal); Writing – review & editing (equal). **Suxing Hu:** Conceptualization (equal); Project administration (equal); Resources (equal); Supervision (equal); Writing – review & editing (equal). **Valeri N. Goncharov:** Conceptualization (equal); Project administration (equal); Resources (equal); Supervision (equal); Writing – review & editing (equal).

DATA AVAILABILITY

The data that support the findings of this study are available from the corresponding author upon reasonable request.

REFERENCES

[1]S. Atzeni and J. Meyer-ter-Vehn, *The Physics of Inertial Fusion* (Oxford Science Publications, 2009).
[2]R. S. Craxton, K. S. Anderson, T. R. Boehly, V. N. Goncharov, D. R. Harding, J. P. Knauer, R. L. McCrory, P. W. McKenty, D. D. Meyerhofer, J. F. Myatt, A. J. Schmitt, J. D. Sethian, R. W. Short, S. Skupsky, W. Theobald, W. L. Kruer, K. Tanaka, R. Betti, T. J. B. Collins, J. A. Delettrez, S. X. Hu, J. A. Marozas, A. V. Maximov, D. T. Michel, P. B. Radha, S. P. Regan, T. C. Sangster, W. Seka, A. A. Solodov, J. M. Soures, C. Stoeckl, and J. D. Zuegel, "Direct-drive inertial confinement fusion: A review," Phys. Plasmas **22**, 110501 (2015).
[3]J. Lindl, "Development of the indirect-drive approach to inertial confinement fusion and the target physics basis for ignition and gain," Phys. Plasmas **2**, 2933 (1995).
[4]R. J. Henchen, M. Sherlock, W. Rozmus, J. Katz, D. Cao, J. P. Palastro, and D. H. Froula, "Observation of nonlocal heat flux using Thomson scattering," Phys. Rev. Lett. **121**, 125001 (2018).
[5]A. L. Milder, H. P. Le, M. Sherlock, P. Franke, J. Katz, S. T. Ivancic, J. L. Shaw, J. P. Palastro, A. M. Hansen, I. A. Begishev, W. Rozmus, and D. H. Froula, "Evolution of the electron distribution function in the presence of inverse bremsstrahlung absorption heating and collisional ionization," Phys. Rev. Lett. **124**, 025001 (2020).
[6]A. L. Milder, J. Katz, R. Boni, J. P. Palastro, M. Sherlock, W. Rozmus, and D. H. Froula, "Measurements of non-Maxwellian electron distribution functions and their effect on laser heating," Phys. Rev. Lett. **127**, 015001 (2021).
[7]D. Turnbull, J. Katz, M. Sherlock, L. Divol, N. R. Shaffer, D. J. Strozzi, A. Colaïtis, D. H. Edgell, R. K. Follett, K. R. McMillen, P. Michel, A. L. Milder, and D. H. Froula, "Inverse bremsstrahlung absorption," Phys. Rev. Lett. **130**, 145103 (2023).
[8]D. Turnbull, J. Katz, M. Sherlock, A. L. Milder, M. S. Cho, L. Divol, N. R. Shaffer, D. J. Strozzi, P. Michel, and D. H. Froula, "Reconciling calculations and measurements of inverse bremsstrahlung absorption," Phys. Plasmas **31**, 063304 (2024).
[9]A. S. Davies, D. Haberberger, J. Katz, S. Bucht, J. P. Palastro, R. K. Follet, and D. H. Froula, "Investigation of picosecond thermodynamics in a laser-produced plasma using Thomson scattering," Plasma Phys. Controlled Fusion **62**, 014012 (2020).
[10]A. B. Langdon, "Nonlinear inverse bremsstrahlung and heated-electron distributions," Phys. Rev. Lett. **44**, 575–579 (1980).
[11]J. P. Matte, M. Lamoureux, C. Moller, R. Y. Yin, J. Delettrez, J. Virmont, and T. W. Johnston, "Non-Maxwellian electron distributions and continuum X-ray emission in inverse Bremsstrahlung heated plasmas," Plasma Phys. Controlled Fusion **30**, 1665–1689 (1988).
[12]M. Sherlock, P. Michel, D. J. Strozzi, L. Divol, E. Kur, and G. Zimmerman, "Inverse bremsstrahlung absorption rate for super-Gaussian electron distribution functions including plasma screening," Phys. Rev. E **109**, 055201 (2024).
[13]J. A. Frenje, R. Florido, R. Mancini, T. Nagayama, P. E. Grabowski, H. Rinderknecht, H. Sio, A. Zylstra, M. G. Johnson, C. K. Li, F. H. Séguin, R. D. Pretrasso, V. Y. Glebov, and S. P. Regan, "Experimental validation of low-*z* ion-stopping formalisms around the Bragg peak in high-energy-density plasmas," Phys. Rev. Lett. **122**, 015002 (2019).
[14]P. J. Adrian, R. Florido, P. E. Grabowski, R. Mancini, B. Bachmann, L. X. Benedict, M. G. Johnson, N. Kabadi, B. Lahmann, C. K. Li, R. D. Petrasso, H. G. Rinderknecht, S. P. Regan, F. H. Séguin, R. L. Singleton, Jr., H. Sio, G. D. Sutcliffe, H. D. Whitley, and J. A. Frenje, "Measurements of ion-electron energy transfer cross section in high-energy-density plasmas," Phys. Rev. E **106**, L053201 (2022).
[15]J. Gonzalez and J. Sheil, "Langdon effect in the realm of extreme ultraviolet source plasmas," Phys. Rev. E **111**, L023201 (2025).
[16]P. Mora and H. Yahi, "Thermal heat-flux reduction in laser-produced plasmas," Phys. Rev. A **26**, 2259 (1982).
[17]C. P. Ridgers, A. G. R. Thomas, R. J. Kingham, and A. P. L. Robinson, "Transport in the presence of inverse bremsstrahlung heating and magnetic fields," Phys. Plasmas **15**, 092311 (2008).
[18]K. Li and W. Y. Huo, "The nonlocal heat transport under the non-Maxwellian distribution in laser plasmas and its influence on laser ablation," Phys. Plasmas **30**, 042702 (2023).
[19]A. V. Maximov, V. P. Silin, and M. V. Chegotov, "Theory of transport in fully ionized plasma," Sov. J. Plasma Phys. **16**, 331 (1990).
[20]V. N. Goncharov and G. Li, "Effect of electric fields on electron thermal transport in laser-produced plasmas," Phys. Plasmas **11**, 5680 (2004).
[21]N. R. Shaffer, A. V. Maximov, and V. N. Goncharov, "Thermal conductivity of a laser plasma," Phys. Rev. E **108**, 045205 (2023).
[22]J. H. Ferziger and H. G. Kaper, *Mathematical Theory of Transport Processes in Gases* (North-Holland, 1972).
[23]E. Fourkal, V. Y. Bychenkov, W. Rozmus, R. Sydora, C. Kirkby, C. E. Capjack, S. H. Glenzer, and H. A. Baldis, "Electron distribution function in laser heated plasmas," Phys. Plasmas **8**, 550–556 (2001).
[24]I. P. Shkarofsy, T. W. Johnston, and M. P. Bachynski, *The Particle Kinetics of Plasmas* (Addison-Wesley, 1966).
[25]A. G. R. Thomas, M. Tzoufras, A. P. L. Robinson, R. J. Kingham, C. P. Ridgers, M. Sherlock, and A. R. Bell, "A review of Vlasov-Fokker-Planck numerical modeling of inertial confinement fusion plasma," J. Comput. Phys. **231**, 1051–1079 (2012).
[26]V. P. Silin, "Nonlinear high-frequency plasma conductivity," Sov. Phys. JETP **20**, 1510 (1965).
[27]V. Perel and Y. M. Pinskii, "Stress tensor for a plasma in a high frequency electromagnetic field with account of collisions," Sov. Phys. JETP **27**, 1014 (1968).
[28]R. D. Jones and K. Lee, "Kinetic theory, transport, and hydrodynamics of a high-Z plasma in the presence of an intense laser field," Phys. Fluids **25**, 2307–2323 (1982).
[29]S.-M. Weng, Z.-M. Sheng, M.-Q. He, H.-C. We, Q.-L. Dong, and J. Zhang, "Inverse bremsstrahlung absorption and the evolution of electron distribution functions accounting for electron–electron collisions," Phys. Plasmas **13**, 113302 (2006).
[30]A. Bendib, K. Bendib-Kalache, B. Cros, and G. Maynard, "Anisotropic electron-distribution function in inverse-bremsstrahlung-heated plasmas," Phys. Rev. E **93**, 043208 (2016).
[31]C. D. Decker, W. B. Mori, J. M. Dawson, and T. Katsouleas, "Nonlinear collisional absorption in laser-driven plasmas," Phys. Plasmas **1**, 4043 (1994).
[32]S.-M. Weng, Z.-M. Sheng, and J. Zhang, "Inverse bremsstrahlung absorption with nonlinear effects of high laser intensity and non-Maxwellian distribution," Phys. Rev. E **80**, 056406 (2009).

[33] A. Bendib, "Nonlinear collisional absorption and induced anisotropy in plasmas heated by an intense laser field," Phys. Plasmas **24**, 070702 (2017).
[34] J. J. Breyt, J. W. Dufty, C. S. Kim, and A. Santos, "Hydrodynamics for granular flows at low density," Phys. Rev. E **58**, 4638 (1998).
[35] L. Spitzer and R. Härm, "Transport phenomena in a completely ionized gas," Phys. Rev. **89**, 977–981 (1953).
[36] E. M. Epperlein, "Kinetic theory of laser filamentation in plasmas," Phys. Rev. Letters **65**, 2145 (1990).
[37] M. Sherlock, J. P. Brodrick, and C. P. Ridgers, "A comparison of non-local electron transport models for laser-plasmas relevant to inertial confinement fusion," Phys. Plasmas **24**, 082706 (2017).
[38] D. Shvarts, J. Delettrez, R. L. McCrory, and C. P. Verdon, "Self-consistent reduction of the Spitzer-Härm electron thermal heat flux in steep temperature gradients in laser-produced plasmas," Phys. Rev. Lett. **47**, 247–250 (1981).
[39] J. F. Luciani, P. Mora, and J. Virmont, "Nonlocal heat transport due to steep temperature gradients," Phys. Rev. Lett. **51**, 1664 (1983).
[40] G. P. Schurtz, P. D. Nicolaï, and M. Busquet, "A nonlocal electron conduction model for multidimensional radiation hydrodynamics codes," Phys. Plasmas **7**, 4238 (2000).
[41] V. N. Goncharov, O. V. Gotchev, E. Vianello, T. R. Boehly, J. P. Knauer, P. W. McKenty, P. B. Radha, S. P. Regan, T. C. Sangster, S. Skupsky, V. A. Smalyuk, R. Betti, R. L. McCrory, D. D. Meyerhofer, and C. Cherfils-Clérouin, "Early stage of implose in inertial confinement fusion: Shock timing and perturbation evolution," Phys. Plasmas **13**, 012702 (2006).
[42] D. Cao, G. Moses, and J. Delettrez, "Improved non-local electron thermal transport model for two-dimensional radiation hydrodynamics simulations," Phys. Plasmas **22**, 082308 (2015).
[43] A. Chrisment, P. Loiseau, J.-L. Feugeas, P.-E. Masson-Laborde, J. Mathiaud, V. Tikhonchuk, and P. Nicholaï, "Analysis of a kinetic model for electron heat transport in inertial confinement fusion plasmas," Phys. Plasmas **29**, 062301 (2022).
[44] H. P. Le, M. Sherlock, and H. A. Scott, "Influence of atomic kinetics on inverse bremsstrahlung heating and nonlocal thermal transport," Phys. Rev. E **100**, 013202 (2019).